



Article

Gravure-Printed Anodes Based on Hard Carbon for Sodium-Ion Batteries

Maria Montanino ^{1,*}, **Claudia Paoletti** ², **Anna De Girolamo Del Mauro** ¹ and **Giuliano Sico** ¹

¹ ENEA—Italian National Agency for New Technologies, Energy and Sustainable Economic Development, Portici Research Centre, Piazzale E. Fermi 1, 80055 Portici, Italy; anna.degirolamo@enea.it (A.D.G.D.M.); giuliano.sico@enea.it (G.S.)

² ENEA—Italian National Agency for New Technologies, Energy and Sustainable Economic Development, Via Anguillarese 301, 00123 Roma, Italy; claudia.paoletti@enea.it

* Correspondence: maria.montanino@enea.it

Abstract: Printed batteries are increasingly being investigated for feeding small, wearable devices more and more involved in our daily lives, promoting the study of printing technologies. Among these, gravure is very attractive as a low-cost and low-waste production method for functional layers in different fields, such as energy, sensors, and biomedical, because it is easy to scale up industrially. Thanks to our research, the feasibility of gravure printing was recently proved for rechargeable lithium-ion batteries (LiBs) manufacturing. Such studies allowed the production of high-quality electrodes involving different active materials with high stability, reproducibility, and good performance. Going beyond lithium-based storage devices, our attention was devoted on the possibility of employing highly sustainable gravure printing for sodium-ion batteries (NaBs) manufacturing, following the trendy interest in sodium, which is more abundant, economical, and ecofriendly than lithium. Here a study on gravure printed anodes for sodium-ion batteries based on hard carbon as an active material is presented and discussed. Thanks to our methodology centered on the capillary number, a high printing quality anodic layer was produced providing typical electrochemical behavior and good performance. Such results are very innovative and relevant in the field of sodium-ion batteries and further demonstrate the high potential of gravure in printed battery manufacturing.



Citation: Montanino, M.; Paoletti, C.; De Girolamo Del Mauro, A.; Sico, G. Gravure-Printed Anodes Based on Hard Carbon for Sodium-Ion Batteries. *Batteries* **2024**, *10*, 407. <https://doi.org/10.3390/batteries10110407>

Academic Editor: Shaokun Chong

Received: 25 October 2024

Revised: 13 November 2024

Accepted: 18 November 2024

Published: 20 November 2024



Copyright: © 2024 by the authors. Licensee MDPI, Basel, Switzerland. This article is an open access article distributed under the terms and conditions of the Creative Commons Attribution (CC BY) license (<https://creativecommons.org/licenses/by/4.0/>).

1. Introduction

The necessity to feed small, portable, and wearable devices increasingly moved the research on printed batteries. Such storage devices, which have a volume below 10 mm^3 and capacity in the range of $5\text{--}10\text{ mAh cm}^{-2}$, must be highly customizable to be perfectly integrated into the device needing the power supply [1]. For this reason, printing technologies were considered a useful manufacturing method, and different techniques were investigated. Printing technologies, in fact, offer the possibility to produce low-cost, thin, flexible, and arbitrary bi-dimensional shapes, different functional layers, and devices (even in the case of multifunctional layered structures), at high throughput, as well as in large areas, with high layer control in terms of homogeneity and thus reproducibility, especially if compared to conventional coating techniques [2]. In fact, coatings are limited in terms of customizability and their main drawback is the low homogeneity of the produced layers, which has consequences on their performances and reproducibility.

In addition, printing technologies are widely investigated for the production of electronic devices. In such cases, the industrial manufacturing of printed batteries could be in-line with the manufacturing of printed electronics in which they have to be inserted. This could result in a great advantage for the economy of the production process.

Printed batteries are already industrially produced, mainly as not-rechargeable primary systems. The most used printing technology, to date, is the screen printing [1].

Among the printing technologies, gravure is very appealing for the production of functional layers, as electrodes for batteries, thanks to its capability to couple high throughput (speed up to 600 m min^{-1}) and high printing quality (resolution $< 2 \mu\text{m}$) [3,4]. In this regard, such a technique can be useful in the study of new materials, when the deposition method is important as the investigated material to obtain its best possible performance. The use of high-performance materials would enable gravure manufacturing for different fields and applications in which large areas are required since it is roll-to-roll compatible. Gravure is widely used in industry for packaging, magazines, and currency; for this reason, each result obtained at a lab scale would be easy to scale up at the industrial level. Moreover, such a technique is highly sustainable, since it has low waste of materials and low energy consumption [5–7]. Despite its many advantages, to date, gravure is few investigated probably because of its main drawback: the use of diluted inks. In fact, an ink suitable for gravure printing has to have a viscosity below 100 mPa . The necessity of diluted ink makes it difficult to obtain a functional layer, especially in the case of composites, and to achieve mass loading useful for practical applications. During the last decade, our studies made an important contribution to the investigation of gravure as a manufacturing method for functional layers, also in the case of electrodes for lithium-ion batteries, improving the comprehension of the process and overcoming some of the most important issues related to the technology [8]. Aiming to rule the formulation of inks suitable for gravure printing, a methodology was recently investigated [9]. Considering the complexity of the process and simplifying its description through the dimensional analysis, the capillary number (Ca) represents the main forces involved during the process:

$$\text{Ca} = \eta U / \gamma \quad (1)$$

where η and γ are the viscosity and the surface tension of the ink, respectively, at a fixed printing speed U . Experimentally, it was proved that when the Ca value is approximatively 1, good printing quality of the layer is achieved and the printed layer is able to display the desired functionality. Each time changing involved materials, different formulations have to be investigated, thus viscosity and surface tension have to be studied to find the best possible ink and the process parameters through the $\text{Ca} = 1$ method. However, our study demonstrated that the printed layer performance also depends on specific issues related to the materials involved in the layer preparation. In the case of electrodes for batteries factors such as mass loading, component ratio, materials size, component distribution, and layer density play a fundamental role in the electrodic performance [8]. Using such methodology, gravure-printed electrodes for lithium-ion batteries (LiBs) were successfully obtained, and high performance was shown when material-specific challenges were addressed [8]. The important results obtained for LiBs motivated our investigation of different storage systems, beyond the lithium chemistry, such as sodium-ion batteries (NaBs). NaBs are widely investigated as alternatives to LiBs due to the abundance and low cost of sodium [10,11]. To date, LiBs are the most investigated and employed storage system for portable and wearable electronic devices, most recently also for electric vehicles and stationary storage systems [12]; however, lithium is expensive and strategic. Na has similar proprieties to Li and the metal ions batteries also operate in a similar way. The NaB mechanism can be described as a reversible migration of Na^+ between the anode and cathode during a charge/discharge process. Recently, sodiated transition metal oxides, phosphates, and organic compounds have been introduced as cathode materials for NaBs; at the same time, studies on anodic materials are carried out, involving carbonaceous materials, transition metal oxides or sulfides, and intermetallic and organic compounds [13].

Na^+ has a radius (1.03 \AA) larger than Li^+ (0.71 \AA), affecting phase stability, transport proprieties, and interphase formation [14]. Due to the different ion sizes, graphite, which is widely employed as an anodic material for LiBs, cannot be used as an anode for NaBs: it has a small interlayered space and tends to form NaC_x too [13]. Most of the investi-

gated active materials for NaBs anodes are not suitable for practical applications due to complex preparation processes [13]. Therefore, advanced anode materials for NaBs, with adequate voltage storage, large reversible capacity, and structural stability, have to be developed to achieve high-performance storage systems. Hard carbon (HC) is a class of carbonaceous materials appealing as an anodic material for NaBs due to their relatively low cost, abundance, and performance [13]. HC structure is different from the ordered layered structure of graphite, consisting of randomly distributed turbostratic domains, containing curved graphene nano-sheets, with expanded interlayer spacing and micro-pores [14]. Such structure is usually obtained through the pyrolysis of a carbon precursor at 1000 °C, obtaining highly branched and cross-linked structure. The branches prevent the ordered graphitization, even pyrolyzing at higher temperatures (up to 3000 °C). The specific value of HC theoretical capacity depends on differences in structure resulting from the synthesis process [14]. Several issues have limited the practical use of HC as an active material for anode manufacturing, such as safety problems related to electroplating and poor cyclability [15]. In this regard, the HC irreversible capacity is the most critical aspect. Such feature depends on several characteristics such as particle sizes, electrolytes, vacancy defects, and porosity [13]. For this reason, further investigation are necessary for boosting the development of HC for NaBs and stabilizing the initial coulombic efficiency. In this paper, the study on a gravure-printed anode for NaBs based on a commercial HC as an active material is reported and discussed. An investigation of the mixing time during the ink preparation was also proposed to evaluate its effect on the electrochemical performance of the active material and of the printed anodes. Sodium-printed batteries were very recently investigated [16]. This is the first example of a gravure-printed anode for NaBs.

2. Materials and Methods

The used active material, hard carbon BHC-300, was provided by MTI Corporation (Richmond, CA, USA). According to the provider, the particle size is in the range of 3–7 μm and the specific surface area is $8 \text{ m}^2 \text{ g}^{-1}$. The inks were prepared using active material (88 wt%), sodium salt of the carboxymethyl cellulose (CMC) (by Dow Wolff Cellulosics (Bomlitz, Germany)) (6 wt%) as a binder, and carbon Super P (by Imerys (Paris, France)) as an electric conductor (6 wt%). The used solvent was a mixture of water and 2-propanol (by Sigma-Aldrich (St. Louis, MO, USA)) (90/10 wt/wt%). Preliminary tests were carried out to determine the best solid content of the ink in terms of viscosity and thus printability. The inks were characterized from a rheological point of view at different temperatures and different shear rates using a Viscotester (by ThermoFisher (Waltham, MA, USA)). The anodic layers were printed on Copper foils pre-treated by Corona (by Tantec (Roskilde, Denmark)). The used lab-scale gravure printer was an IGT-G1-5 (Almere, The Netherlands) equipped with a cylinder with a line density of 40 lines cm^{-1} , a stylus angle of 120°, a cell depth of 72 μm , and a screen angle of 53°. To increase the thickness and the mass loading of the printed anodes, a multilayer approach was adopted, printing 10 and 15 consecutive layers, one on each other, overlapping the same ink at the same printing conditions. Between each printed layer, a fast dryer was performed using a blow of air. The layers were printed at a speed of 36 m min^{-1} and a printing force of 700 N and finally dried at 100 °C for 1 h. Printed anodes were morphologically investigated using scanning electron microscopy (Zeiss (Jena, Germany); LEO 1530) and electrochemically characterized in half cells versus metallic Na. The cells were prepared using glass fiber separators (by Whatman (Maidstone, UK) and a 1 M solution of NaClO_4 (by Sigma-Aldrich) in propylene carbonate by Fluka (Charlotte, NC, USA) as electrolyte. Galvanostatic cycling measurements were performed on the cells using a Maccor 4000 (Tulsa, OK, USA) at 20 °C and fixed 0.1 C rate.

3. Results and Discussion

The gravure process consists of the direct transfer of ink from the engraved cells of a printing cylinder onto a flexible substrate thanks to the pressure of a counter cylinder, as depicted in Figure 1.

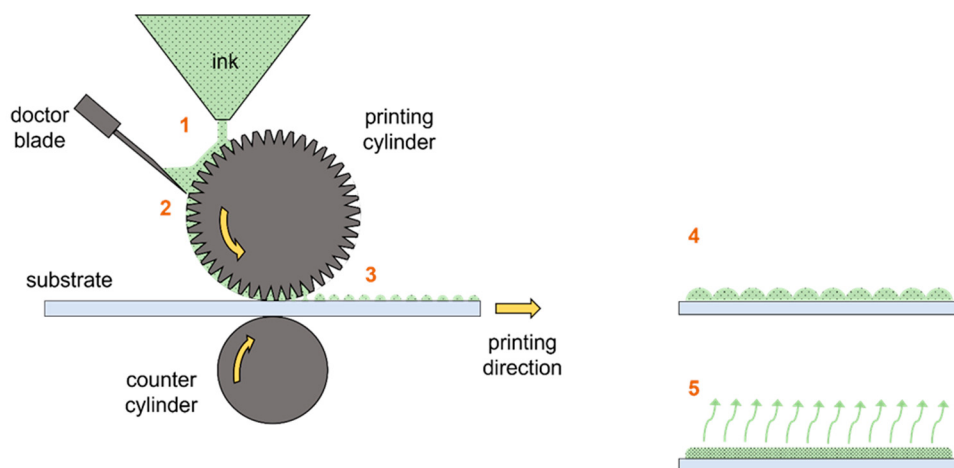


Figure 1. Operating roll-based gravure printing principle, showing inking (1), doctoring (2), transfer (3), spreading (4), and drying (5) sub-processes. Adapted with permission from Ref. [8].

Printing quality depends on several parameters related to the following: a. Gravure cylinder, such as cell geometry, cell density, surface energy, and diameter; b. Process, such as printing speed, printing force, and web tension; c. Ink, such as viscosity, surface tension, solvent evaporation rate, and solid content; d. Substrate, such as surface energy, roughness, and porosity. The process can be described as a series of sub-processes: 1. Inking, by filling the engravings of the printer cylinder with ink; 2. Doctoring, by removing the excess of ink from the printing cylinder; 3. Transfer of ink onto the flexible substrate; 4. Spreading, through the coalescence of ink droplets onto the substrate; 5. Drying, by completely removing the solvent. Each of such stages has its own ideal regime and all of them concur to determine the final printing quality [17]. The gravure process is very complex from the fluid-dynamic point of view and is not easy to model. The dimensionless analysis can help to simplify the process description and study through the capillary number. The ink formulation has a key role in the printing process; the Ca methodology was adopted to determine the best and most useful ink characteristics for the formulation and the process.

Experimentally, several inks containing different solid contents were prepared and rheologically tested to verify their Newtonian behavior. The solid content was chosen to give a viscosity below 100 mPa s. Among the inks respecting such requirements, we chose the one with the highest solid content. After determining the ink viscosity and its surface tension, Ca values were calculated at different printing speeds, selecting the practical one in a way to maximize the speed and contemporarily obtain a Ca value approaching the unity. The necessity to maximize the printing speed belongs to the idea of approaching the industrial conditions, minimizing time and cost. The research was also devoted to decreasing the amount of electric conductors and polymers in the final layer. The sustainability of the process and the products was enhanced through the use of water as a prevalent solvent since a water-soluble binder, carboxymethyl cellulose, was used in the ink composition. A small amount of 2-Propanol was used as a co-solvent to decrease the high ink surface tension due to the use of water (from 72 to 42 mN m⁻¹) and make the ink printable with a surface tension lower than the surface energy of the printing cylinder and of the substrate [8]. The ink was prepared by keeping the relative ratio of the solid components constant and changing the total solid amount.

The tested solid contents were 18, 15, and 14 wt%. The prepared inks were rheologically tested and all of them showed a Newtonian behavior (see Figure 2), namely, having a viscosity independent of the shear rate; the representative value of viscosity, at shear rate 100 s⁻¹, for the tested inks is reported in Table 1.

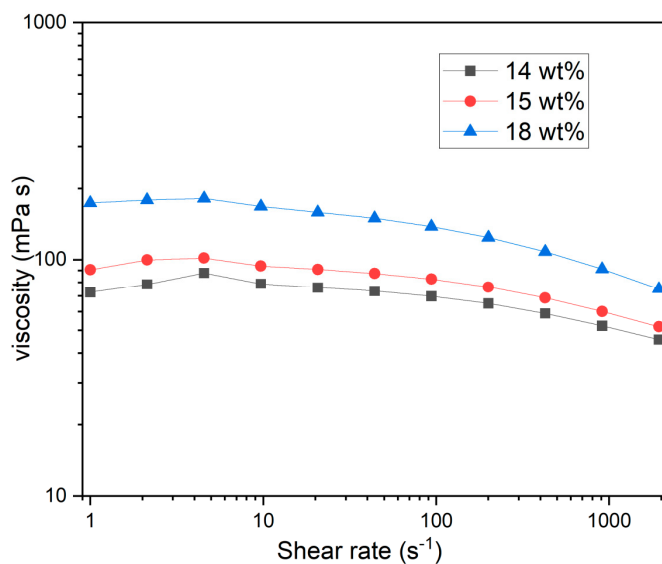


Figure 2. Viscosity versus shear rate for the prepared inks at different solid content (14, 15, 18 wt%).

Table 1. Viscosity and Ca for the inks at different solid content.

Solid Content (wt%)	Viscosity @ 20 °C (mPa s)	Printing Speed (m s^{-1})	Ca
18	138	0.6	1.97
		0.4	1.31
		0.2	0.66
15	83	0.6	1.18
		0.4	0.80
		0.2	0.40
14	70	0.6	1.00
		0.4	0.67
		0.2	0.34

To achieve high printing quality, we proposed a methodology mainly based on the capillary number approaching the unity [8]. In Table 1, the calculated values of Ca were reported for the inks at different solid contents.

The Ca was determined considering the surface tension of the solvent (42 mN m^{-1}) [18]. The choice of the printing speed follows the calculation of the Ca based on the measurements of ink viscosity and surface tension. The best possible ink is the one with suitable viscosity for gravure (below 100 mPa s) and the highest possible solid content, which combined with the printing speed brings a $\text{Ca} = 1$. In other words, the choice is based on a compromise to maximize both the solid content and the printing speed (for industrial reasons), achieving the $\text{Ca} = 1$ target. Higher speeds are possible; however, they require lower viscosity, namely, lower solid content of the ink, decreasing the mass loading of the printed layer, thus requiring a higher number of layers to be overlapped. The investigated inks, reported in Table 1, show that the 18 wt% ink had a viscosity out of the gravure printing range. Regarding the 15 wt% ink, the 0.4 m s^{-1} speed was not preferred in the view of speed maximization, while the 0.6 m s^{-1} speed gave a Ca higher than the one obtained at the same speed for the 14 wt% ink. Such excess on the Ca favors viscous forces over surface tension, causing possible pin-holes or void formation due to a lower ink spreading. For all such reasons, the 14 wt% ink was selected to realize the printed layer as the best compromise and was printed at 0.6 m s^{-1} and at a printing force of 700 N. Different ball milling time treatments were tested on the selected ink to investigate the homogenization of the particle sizes and distribution: 15 min, 60 min, and 3 h. All the inks were printed overlapping ten layers, while the ink ball milled for three hours was printed overlapping 15 layers too. All the printed samples showed high printing quality, and thus

good coverage and homogeneity, without critical defects, such as voids and scratches, as shown by the SEM images (see Figures 3 and 4).

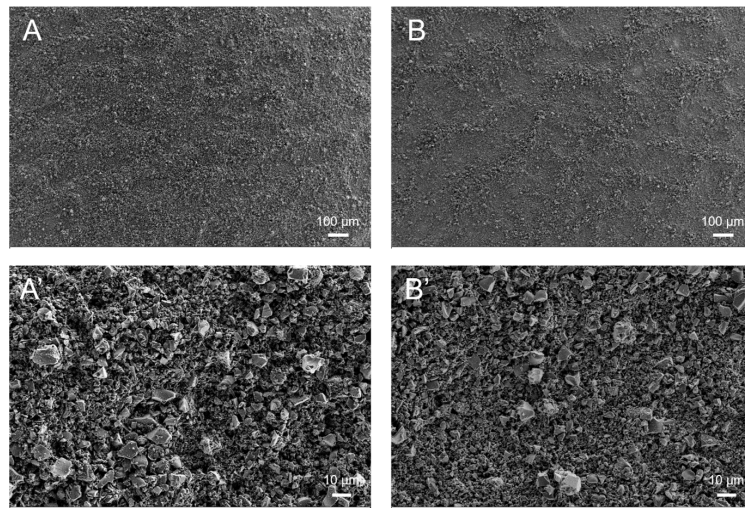


Figure 3. SEM images of the gravure printed layers: 15 min ball-milled ink (**A,A'**) and 60 min ball milled (**B,B'**) at different magnifications.

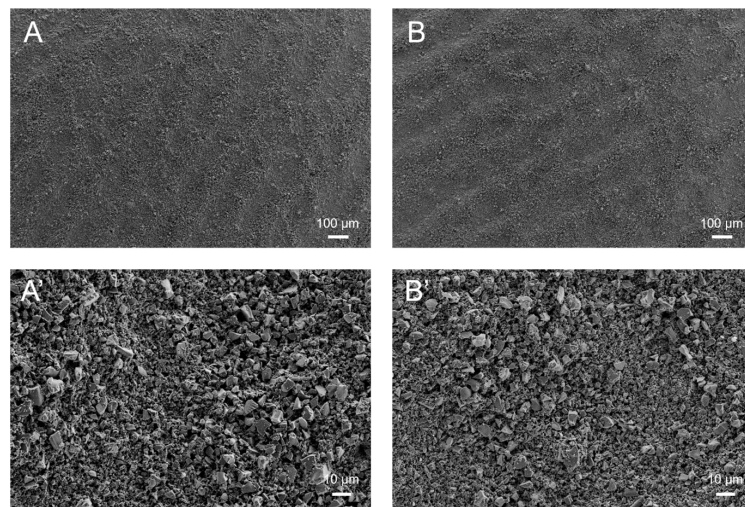


Figure 4. SEM images of the gravure printed layers: 3 h ball-milled ink overlapping 10 layers (**A,A'**) and 15 layers (**B,B'**) at different magnifications.

Sixty-minute ball milling increased the layer homogeneity decreasing the differences in particle size (see Figure 3). Further increase in ball milling time, up to 3 h, further increased the homogeneity of printed layers, as it is possible to notice by comparing the B, B' images in Figure 3 and A, A' images in Figure 4. When 15 layers of ink were overlapped instead of 10 layers, working at fixed printing parameters, a slight worsening in the printed layer quality can be observed (see Figure 4). The characteristics of the 10 printed layers are reported in Table 2.

Table 2. Characteristics of the printed layer, obtained by using different inks and calculated apparent density [19].

Ink/BM Time	Mass Loading (mg cm ⁻²)	Active Material (mg cm ⁻²)	Thickness (cm)	Apparent Layer Density (g cm ⁻³)
15 min	0.80	0.70	2.6×10^{-3}	0.31
60 min	0.94	0.83	2.6×10^{-3}	0.36
3 h	0.92	0.81	2.0×10^{-3}	0.46

The increase in homogeneity of particle size with the increase in the ball milling time provoked a better packing of the materials in the printed layer, which is proved by the increase in apparent layer density from 0.31 to 0.46 g cm⁻³.

The printed layers were characterized from the electrochemical point of view in half cell versus Na displaying anodic functionality. In Figure 5 voltage vs. specific capacity curves are reported for the discharge process of selected cycles of 10-layer anodes obtained by using 15 min and 3 h ball-milled inks. Such trends were typical of the sodiation-desodiation process occurring in the HC-based anode, showing adsorption/desorption of Na⁺ at high potential and the reversible intercalation/deintercalation process, resulting in a plateau at low potential [20]. The 10-layer printed anode obtained using 15 min ball-milled ink showed an irreversible capacity in the range of 400–440 mAh g⁻¹ for the first 20–30 cycles, following a drop in capacity to 130 mAh g⁻¹, as can be observed in Figure 6. The reversible capacity of 130 mAh g⁻¹ was stable up to 100 cycles cycling at a fixed 0.1 C rate, without fading yet. The anodes printed using inks ball-milled for longer times (60 min and 3 h) did not show irreversible behavior, having from the beginning a reversible capacity of about 120 mAh g⁻¹, stable over 100 cycles at a fixed 0.1 C rate. In Figure 6, the specific capacity behavior of the printed layer obtained using 3 h ball-milled ink was reported as an example. The 15-layer gravure printed anode obtained with the 3 h ball-milled ink showed similar electrochemical behavior to the 10-printed-layer anode obtained with the same ink but displayed a lower specific capacity (90 mAh g⁻¹).

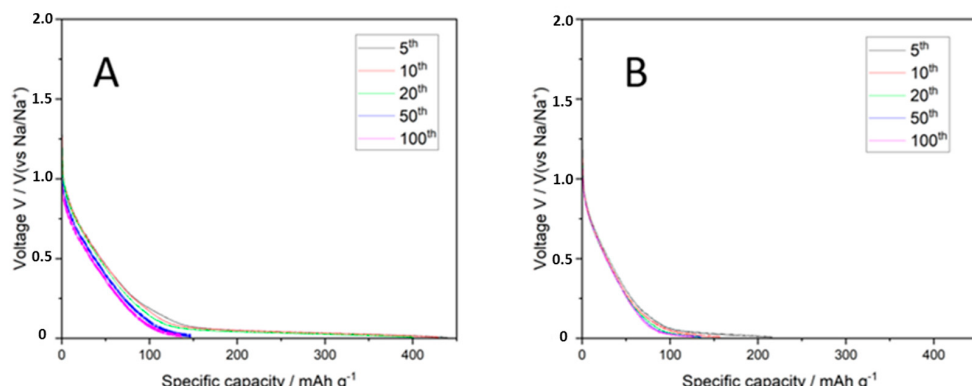


Figure 5. Voltage vs. specific capacity in discharge for gravure printed electrodes based on HC obtained using ball-milled inks at 15 min (**A**) and 3 h (**B**) for selected cycles (5th, 10th, 20th, 50th, 100th).

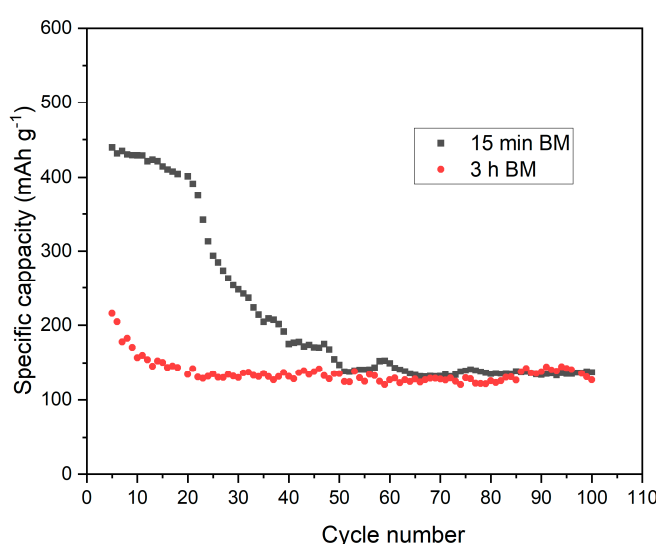


Figure 6. Discharge-specific capacity for gravure printed electrodes based on HC obtained using ball-milled inks at 15 min and 3 h.

The Na^+ storage mechanism for the HC is still under debate. According to the most recent results, this process can be described by a three-step insertion model: Na^+ ions are adsorbed on the defects of the HC-based anodic layer, then the Na^+ is intercalated in the HC structure and finally adsorbed onto the pore surface [21]. On such a basis, the obtained electrochemical results can be explained by considering the HC structure in the investigated gravure printed anodic layers. In fact, HC is composed of pseudo-graphitic and amorphous regions, which can be represented as a “house of cards” model, including a large number of defects, voids, and pores [11]. Due to such morphology a part of Na^+ forms clusters which are irreversibly trapped into the HC layers. The trapped sodium is not released in the subsequent de-sodiation process due to the strong interaction occurring between the graphene sheets, decreasing the sodium taking part in the redox process and causing the loss of Coulombic efficiency. This phenomenon, together with the Na^+ involved in the solid electrolyte interface (SEI) formation, causes a decrease in electrochemical performance leading to the irreversible fraction of capacity. Most likely, the prolonged ball-milling treatment is able to modify the HC structure affecting the charge/discharge process and dramatically cutting the irreversible part of the capacity. This could be the reason why the specific capacity results lower (from 400 to 120 mAh g^{-1}) since the first cycle. However, the capacity remains stable over a hundred cycles, demonstrating the high stability of the active material and the anode itself. Future works for enhancing the performances of the gravure printed anodes based on HC may aim for the stabilization of the HC structure within the printed layer, e.g., suitably tuning the porosity.

4. Conclusions

In this work, the feasibility of employing HC as an active material for Na-ion batteries in an anodic layer produced by gravure printing was investigated. The HC-based gravure printed anode is able to display up to 440 mAh g^{-1} . However, the intrinsic characteristic of the active material leads to a decrease in charge/discharge capacity, showing an irreversible part of capacity. The prolonged ball-milling of the ink probably affects the morphology of the printed anode, cutting out the irreversible part of the specific capacity, displaying about 120 mAh g^{-1} . Nevertheless, the displayed capacity remains unchanged over a hundred cycles, proving the stability of the active material and of the printed anode. On the base of such findings, further work can be employed to stabilize the HC structure in the printed layer, investigating the effect of porosity and/or reducing the defects.

Author Contributions: Conceptualization, M.M. and G.S.; methodology, M.M., A.D.G.D.M., C.P. and G.S.; validation, M.M. and G.S.; formal analysis, M.M. and G.S.; investigation, M.M., A.D.G.D.M., C.P. and G.S.; resources, M.M.; data curation, M.M. and G.S.; writing—original draft preparation, M.M.; writing—review and editing, M.M. and G.S.; visualization, M.M., A.D.G.D.M. and G.S.; supervision, M.M. and G.S.; funding acquisition, M.M. All authors have read and agreed to the published version of the manuscript.

Funding: This research was funded by Ministry of the Environment, grant number I53C22003080001, by Accordo di Programma 2022–2024 Progetto di ricerca integrato: Tecnologie di accumulo eletrochimico e termico; WP1-Accumulo eletrochimico: materiali avanzati.

Data Availability Statement: The raw data supporting the conclusions of this article will be made available by the authors upon request.

Conflicts of Interest: The authors declare no conflicts of interest.

References

1. Oliveira, J.; Costa, C.M.; Lanceros-Méndez, S. *Printed Batteries Materials, Technologies and Applications*; John Wiley & Sons Ltd.: Chichester, UK, 2018; pp. 1–14.
2. Krebs, F.C. Fabrication and processing of polymer solar cells: A review of printing and coating techniques. *Sol. Energy Mater. Sol. Cells* **2009**, *93*, 394–412. [[CrossRef](#)]
3. Grau, G.; Kitsomboonloha, R.; Subramanian, V. Fabrication of a high-resolution roll for gravure printing of 2 μm features. In Proceedings of the SPIE Organic Photonics + Electronics, San Diego, CA, USA, 9–13 August 2015.

4. Tiara, A.M.; Moon, H.; Cho, G.; Lee, J. Fully roll-to-roll gravure printed electronics: Challenges and the way to integrating logic gates. *Jpn. J. Appl. Phys.* **2022**, *61*, SE0802.
5. Søndergaard, R.R.; Hosel, M.; Krebs, F.C. Roll-to-Roll Fabrication of Large Area Functional Organic Materials. *J. Polym. Sci. Part B Polym. Phys.* **2013**, *51*, 16–34. [[CrossRef](#)]
6. Khan, S.; Lorenzelli, L.; Dahiya, R. Technologies for printing sensors and electronics over large flexible substrates: A review. *IEEE Sens. J.* **2015**, *15*, 3164–3185. [[CrossRef](#)]
7. Huang, Q.; Zhu, Y. Printing conductive nanomaterials for flexible and stretchable electronics: A review of materials, processes, and applications. *Adv. Mater. Technol.* **2019**, *4*, 1800546. [[CrossRef](#)]
8. Montanino, M.; Sico, G. Gravure Printing for Lithium-Ion Batteries Manufacturing: A Review. *Batteries* **2023**, *9*, 535. [[CrossRef](#)]
9. Montanino, M.; Paoletti, C.; De Girolamo Del Mauro, A.; Sico, G. The Influence of the Gravure Printing Quality on the Layer Functionality: The Study Case of LFP Cathode for Li-Ion Batteries. *Coatings* **2023**, *13*, 1214. [[CrossRef](#)]
10. Yabuuchi, N.; Kubota, K.; Dahbi, M.; Komada, S. Research development on sodium-ion batteries. *Chem. Rev.* **2014**, *114*, 11636. [[CrossRef](#)] [[PubMed](#)]
11. Slater, M.D.; Kim, D.; Lee, E.; Johnson, C.S. Sodium-ion batteries. *Adv. Funct. Mater.* **2013**, *23*, 947. [[CrossRef](#)]
12. Scrosati, B.; Garche, J. Lithium batteries: Status, prospects and future. *J. Power Sources* **2010**, *195*, 2419–2430. [[CrossRef](#)]
13. Yang, Y.; Wu, C.; He, X.-X.; Zhao, J.; Yang, Z.; Li, L.; Wu, X.; Li, L.; Chou, S.-L. Boosting the development of hard carbon for sodium-ion batteries: Strategies to optimize the initial coulombic efficiency. *Adv. Funct. Mater.* **2024**, *34*, 2302277. [[CrossRef](#)]
14. Xiao, B.; Rojo, T.; Li, X. Hard carbon as Sodium-ion battery anodes: Progress and challenges. *ChemSusChem* **2019**, *12*, 133–144. [[CrossRef](#)] [[PubMed](#)]
15. Hasegawa, G.; Kanamori, K.; Kannari, N.; Ozaki, J.-I.; Nakanishi, K.; Abe, T. Hard carbon anodes for Na-ion batteries: Toward a practical use. *ChemElectroChem* **2015**, *2*, 1917–1920. [[CrossRef](#)]
16. Ren, H.; Zhang, X.; Liu, Q.; Tang, W.; Liang, J.; Wu, W. Fully-printed flexible aqueous rechargeable sodium-ion batteries. *Small* **2024**, *20*, 2312207. [[CrossRef](#)] [[PubMed](#)]
17. Sico, G.; Montanino, M.; Pronteria, C.T.; De Girolamo Del Mauro, A.; Minarini, C. Gravure printing for thin film ceramics manufacturing from nanoparticles. *Ceram. Int.* **2018**, *44*, 19526–19534. [[CrossRef](#)]
18. Vázquez, G.; Alvarez, E.; Navaza, J.M. Surface Tension of Alcohol + Water from 20 to 50 °C. *J. Chem. Eng. Data* **1995**, *40*, 611–614. [[CrossRef](#)]
19. Montanino, M.; De Girolamo Del Mauro, A.; Paoletti, C.; Sico, G. Gravure Printing of Graphite-Based Anodes for Lithium-Ion Printed Batteries. *Membranes* **2022**, *12*, 999. [[CrossRef](#)] [[PubMed](#)]
20. Morikawa, Y.; Nishimura, S.-I.; Hashimoto, R.-I.; Ohnuma, M.; Yamada, A. Mechanism of sodium storage in hard carbon: An X-ray scattering analysis. *Adv. Energy Mater.* **2020**, *10*, 1903176. [[CrossRef](#)]
21. Hwang, J.-Y.; Myung, S.-T.; Sun, Y.-K. Sodium-ion batteries: Present and future. *Chem. Soc. Rev.* **2017**, *46*, 3529. [[CrossRef](#)] [[PubMed](#)]

Disclaimer/Publisher’s Note: The statements, opinions and data contained in all publications are solely those of the individual author(s) and contributor(s) and not of MDPI and/or the editor(s). MDPI and/or the editor(s) disclaim responsibility for any injury to people or property resulting from any ideas, methods, instructions or products referred to in the content.